{113} Twinned ZnSe Bicrystal Nanobelts Filled with <111> Twinnings

Lei Jin,[†,‡,§] Jianbo Wang,*,[†,‡] Guangyi Cao,[†,‡] Zhongling Xu,[†,‡] Shuangfeng Jia,[†,‡] Wallace C. H. Choy,*,[§] Yee P. Leung,[§] and Tong I. Yuk[§]

Department of Physics and Center for Electron Microscopy, Wuhan University, Wuhan 430072, China, Key Laboratory of Acoustic and Photonic Materials and Devices of Ministry of Education, Wuhan University, Wuhan 430072, China, and Department of Electrical and Electronic Engineering, University of Hong Kong, Pokfulam Road, Hong Kong, China

Received: November 12, 2007; In Final Form: February 1, 2008

Zinc selenide (ZnSe) bicrystal nanobelts with zinc blende structure were obtained via simple thermal evaporation of ZnSe powder and were further investigated by various transmission electron microscopy (TEM) techniques. The bicrystal nanobelts form by introducing {113} twinning. It is interesting to note that the commonly found <111> twinning lamellas, with width ranging from 5 to 30 nm, concurrently grow in each single plate of the bicrystal nanobelts. The crystallographic relations of the ZnSe bicrystal nanobelts are comprehensively characterized by using selected area electron diffraction analysis and high-resolution TEM. The polarity around the twin planes are determined by convergent beam electron diffraction technique, which indicates the absence of polarity reversal along <111> direction. By taking account of the polarity of zinc blende ZnSe, the atomic model and the growth mechanism are also discussed. This novel structure provides a model system for further study of its mechanical, electrical, and optical properties.

1. Introduction

One-dimensional (1D) nanostructures, which are considered to be ideal building blocks of functional nanoscale devices, have attracted extraordinary attention for their applications.[1] Considerable efforts have been devoted to fabricating various 1D nanostructures, as well as achieving well-defined interfaces induced by structural modulations.[2−9] Zinc selenide (ZnSe), with the bulk-crystal energy band gap of 2.7 eV at 300 K,[10] exhibits a great potential for various optoelectronic devices, including blue-green laser diodes, light emitting diodes, etc.[11] It is also a key material for applications in spintronics[12] and used as a window in the infrared region.[13] ZnSe-based microstructures have been widely investigated in recent years. By using the thermal evaporation method, we have previously reported the growth of ZnSe nanorings,[4] triple-crystal nanobelts,[5] and abnormal nanowheels[6] with a wurtzite metastable phase.

On the other hand, as one of the most significant defects, twinning could generate positive energy and consequently is expected to have important influence on the mechanical, electronic, and optical properties of material.[7−8,14] Actually, investigations show that the twin boundary can evidently function as a natural potential well for electrons, thus inducing a two-dimensional (2D) electron system which exhibits different physical properties.[14] For a better understanding of the performance of nanostructures, it becomes imperative to investigate the defect configurations down to atomic level. <111> twinning is one of the structures that are commonly found in cubic system. Nanowires with alternating twins along the <111> direction
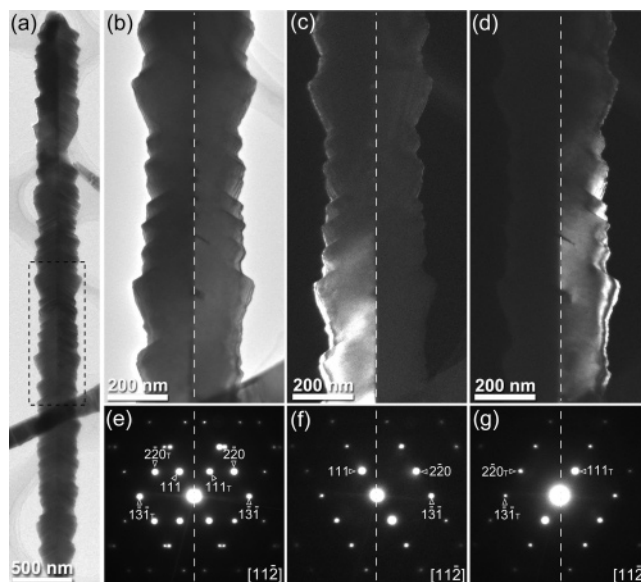

Figure 1. (a) BF TEM image of a typical ZnSe bicrystal nanobelt. (b) An enlarged BF image and (e) the SAED pattern from the area in the black frame in a. (c,d) The corresponding DF TEM images. (f,g) The corresponding SAED patterns. The dashed line indicates the twinning plane.

have been widely reported in ZnSe,[3] GaP,[9] and indium doped ZnO,[8] and <111> twinning in Cu₂O quantum dots has also been studied at the atomic level.[15] Besides, the two kinds of commonly detected twin boundaries are tricrystalline and bicrystalline nanostructures. Bicrystal nanobelts (or nanoribbons), which are composed of two nanobelts (or nanoribbons) connected by a twinning plane, have been widely used in microelectronics for enhancing operation efficiency and acting as an intermediate for the fabrication of other devices, such as single Josephson's junctions and colossal magnetoresistance

* Author to whom correspondence should be addressed. E-mail: wang@ whu.edu.cn (J.W.) and chchoy@eee.hku.hk (W.C.H.C.).
  † Department of Physics and Center for Electron Microscopy, Wuhan University.
  ‡ Key Laboratory of Acoustic and Photonic Materials and Devices of Ministry of Education, Wuhan University.
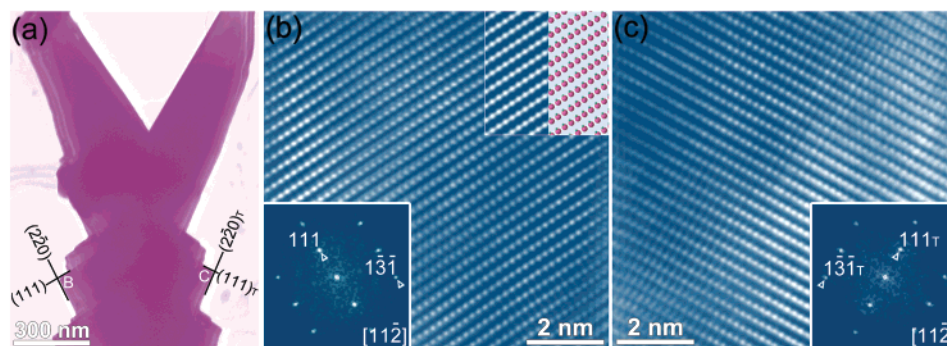 § University of Hong Kong.

Figure 2. (a) BF TEM image of a ZnSe bicrystal nanobelt. (b,c) HRTEM images taken from the area labeled by B and C shown in a. The insets are the FFT patterns (bottom) and HRTEM simulation image with and without atomic model superimposed (top).

devices.[16] Different bicrystalline nanobelts including ZnO, ZnS, In_2O_3, β-Ga_2O_3, and so forth have been obtained,[17] but there is no previous report about the ZnSe bicrystalline nanostructures.

Herein, we report a zinc blende structured ZnSe bicrystal nanobelt with a twinning in the uncommonly observed {113} plane. It is interesting to note that the widely reported <111> twinnings are concurrently embedded in each plate of the as-synthesized bicrystal nanobelts. Structural investigations, including selected area electron diffraction (SAED) and high-resolution transmission electron microscopy (HRTEM), have been performed as in section 3.1 to ascertain the crystallographic relations around the twin boundaries. In section 3.2, the convergent beam electron diffraction (CBED) method has been applied to determine the absolute polarity, which indicates the absence of polarity reversal along <111> direction and is expected to effect the nanobelt growth. On the basis of the polarity result, an atomic model is constructed, which may contribute to further understanding of the performance of this novel nanostructure. Finally, the formation of the bicrystal nanobelts is discussed in section 3.3, and some conclusions are drawn in section 4.

2. Experimental Section

The ZnSe bicrystal nanobelts were grown in a tube furnace. About 0.5 g ZnSe powder (99.99% Sigma Aldrich) was loaded in an alumina boat and pushed into the center of the furnace. The silicon (100) substrate, coated with ~5 nm of gold film, was placed 30 cm downstream from the source. The furnace was then pumped to ~0.07 Torr and purged with the carrier gas of high-purity argon premixed with 5% hydrogen at a rate of about 200 sccm (sccm denotes standard cubic centimeters per minute) to remove the residual oxygen. After that the flow rate of the carrier gas was maintained at 200 sccm and the pressure was set at 100 Torr. The furnace was then heated up to 950 °C and maintained for 60 min. After a 35 min growth, the pressure was changed immediately to 0.02 Torr. After the growth, the furnace was cooled down naturally to room temperature. Yellowish products were obtained on the substrate.

The products were then scratched off the substrate and sonicated in ethanol, then dropped onto the holey carbon-coated copper grid for transmission electron microscopy (TEM) observation. TEM observations including bright field (BF) imaging, dark field (DF) imaging and SAED were performed using JEOL JEM-2010(HT) electron microscope, CBED patterns and HRTEM characterizations were taken on JEOL JEM-2010FEF(UHR) electron microscope equipped with field emission gun and Ω-type in-column energy filter system. Both microscopes were operated at the acceleration voltage of 200 kV.

3. Results and Discussion

3.1. Morphology of ZnSe Bicrystal Nanobelts. Figure 1a shows a BF image of a typical ZnSe bicrystal nanobelt with width of ~400 nm and length of several micrometers. It is interesting to note that the ZnSe bicrystal nanobelt shows a high degree of mirror symmetry between two sides and a spine can also be clearly observed. Figure 1b presents an enlarged view of the portion marked by a black frame in Figure 1a, which is projected along the [11$\bar{2}$] direction. It demonstrates that the contrasts of both sides are nearly the same. The corresponding SAED pattern shown in Figure 1e is of the zinc blende structure but with twinning in the ($\bar{1}$3$\bar{1}$) plane (see the dashed line) and is superimposed by the patterns corresponding to the single crystals on both sides of the twinning (as indexed). Further calculations based on series of experimental SAED patterns and as-observed length of the bicrystal nanobelt (not shown) indicate that the belt lies horizontally on the copper grid while the incident electron beam is along the [11$\bar{2}$] axis. Hence, the growth direction of the bicrystal nanobelt is [7$\bar{1}$4], which is perpendicular to the [11$\bar{2}$] axis and in the ($\bar{1}$3$\bar{1}$) plane. DF images as shown in Figure 1c,d are taken from the same portion of the nanobelt, and the corresponding SEAD patterns are present in Figure 1f,g, respectively. It seems that each single part of the bicrystal nanobelt consists of single crystalline ZnSe, according to the SAED patterns.

The bicrystal nanobelt is further characterized by HRTEM. Figure 2a is the BF image, and the HRTEM images are shown in Figure 2b,c, which corresponds to the areas labeled with B and C in Figure 2a, respectively. Corresponding fast Fourier transformed (FFT) patterns are inserted in Figure 2b,c (bottom), which are consistent with the SAED patterns in Figure 1f,g, respectively. HRTEM simulation is carried out using JEOL MssC software, and the atomic model is also superimposed in Figure 2b, which fits the experimental result well.

In order to intuitively illustrate the twin variants, tilting technique is indispensable. The BF image is shown in Figure 3a. It can be seen that the two parts of the nanobelt display different contrasts, which are indicated by the dashed line. Moreover, a black−white striped contrast (as marked by the arrowheads) is remarkable which is obviously different from that shown in Figure 1b. A zoomed-in BF image is presented in Figure 3b after tilting; we can also observe the black−white stripes, whose widths are nearly in the region from 5 to 30 nm. The SAED pattern, taken from the region labeled by C, is shown in Figure 3c and confirms the cubic ZnSe structure. However, it contains twinnings along the <111> axis which is viewed along the [10$\bar{1}$] axis. Further analysis shows that the angle between (1$\bar{1}$1) and (1$\bar{1}$1)$_T$ planes is ~140.6°.

{113} Twinned ZnSe Bicrystal Nanobelts

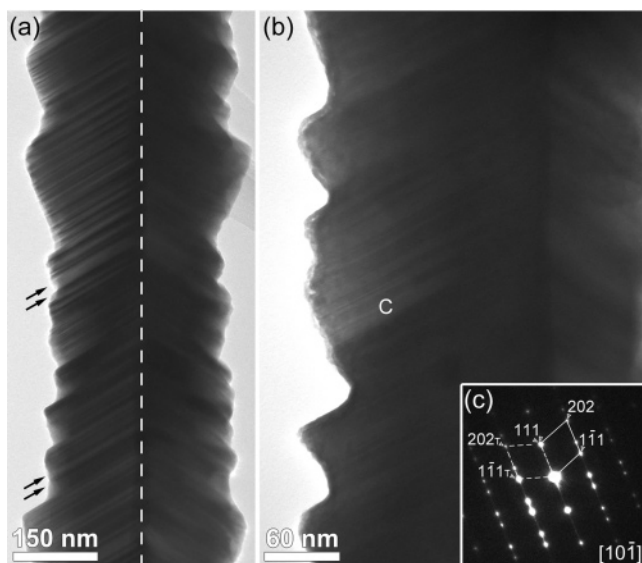*J. Phys. Chem. C, Vol. 112, No. 13, 2008* **4905**

Figure 3. (a) BF image of the nanobelt after slightly tilting. (b) A zoomed-in BF image of the nanobelt showing black-white striped contrast. (c) Corresponding SAED pattern taken from the area labeled by C in b.
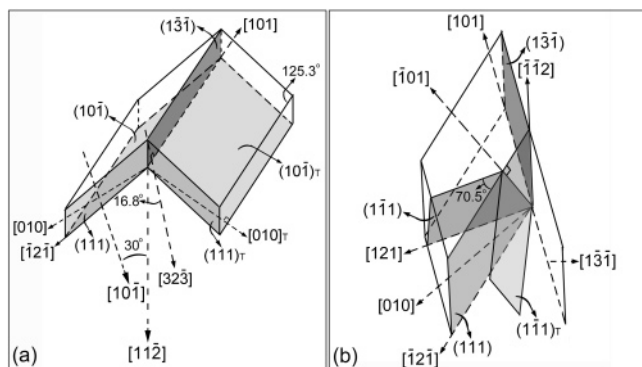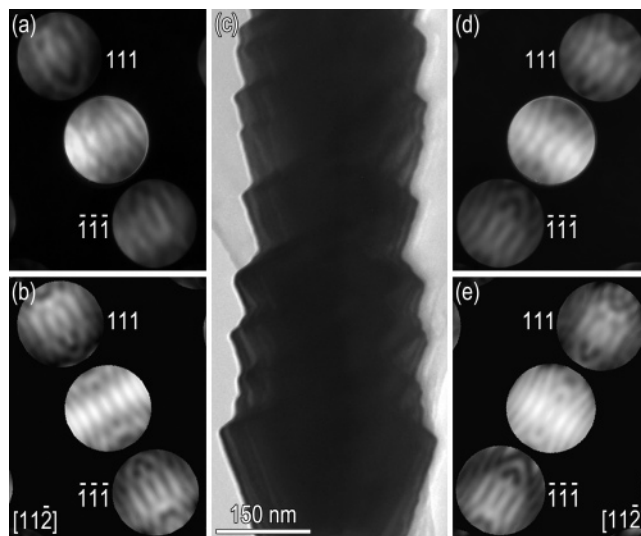

Figure 5. BF image and corresponding CBED patterns of a ZnSe bicrystal nanobelt projected along [11$\bar{2}$] axis. (c) BF image. (a,d) Experimental CBED patterns recorded from the left and right part, respectively. (b,e) Simulated CBED patterns corresponding to a and d, respectively.


Figure 4. Schematic illustrations of (a) the ZnSe bicrystal nanobelt and (b) a single part showing the crystallographic relations.

Thus, a novel ZnSe {113} twinned bicrystal nanobelt, which is filled with nanoscale <111> twinning lamellas, is observed. As for the <111> twinning, it has been widely reported in refs 3, 8, 9, and 15, and the electronic properties of confined electrons at naturally formed {111} twin boundaries have been investigated, showing a 2D character.[14] However, there are limited reports on the compound twinning structure consisting of {113} twinning concurrently filled with <111> lamellar twinnings in the face-centered cubic (fcc) structures. Analogously, rod-like defects (RLD) forming on the {111} and {113} habit planes have been observed in silicon and fully characterized by TEM, which are proved to have both electrical and optical activities.[18] In order to demonstrate the crystallographic relations of the ZnSe bicrystal nanobelts, we draw the schematic illustration as Figure 4 from the above experimental determination.

Figure 4a illustrates the relations between the crystallographic facets and the axes of the typical ZnSe bicrystal nanobelt. It forms by introducing twinning in the ($1\bar{3}1$) plane to connect both parts of the nanobelt. The angle between the ($10\bar{1}$) and ($10\bar{1}$)$_T$ planes is 129.5° which is twice that between [3$\bar{2}$3] and [010] axes. As for a single part, schematic illustration is also presented in Figure 4b. The <111> twinning forms, and the angle between ($1\bar{1}1$) and ($1\bar{1}1$)$_T$ is 141° on the basis of the
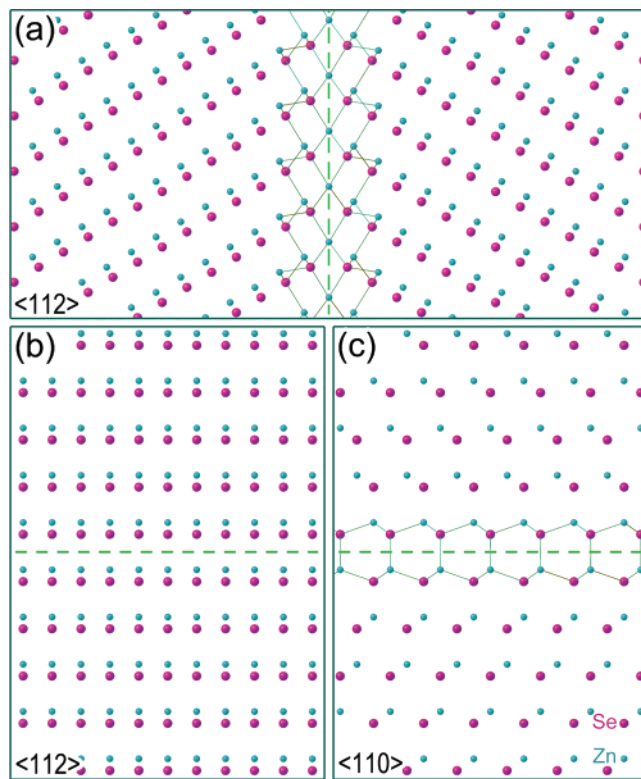
Figure 6. Atomic model of the ZnSe {113} bicrystal nanobelt filled with <111> twinnings. (a) Projection along <112> axis showing {113} mirror twinning. (b) Projection of the single part along <112> axis with 180° rotation twinning veiled. (c) Projection of the single part along <110> axis with 180° rotation twinning unveiled.

crystallographic calculation which is consistent with the TEM measurement in Figure 3c.

3.2. Polarity and Atomic Model. Owing to the structurally noncentral symmetry of the zinc blende structure, two types of twinnings can form: the so-called orthotwin and paratwin. The orthotwin is obtained by 180° rotation around <111> crystallographic axis, while the latter forms by mirror reflection about the twinning plane.[19] As a result, the polarity will reverse when crossing the paratwin while it will stay unchanged when crossing
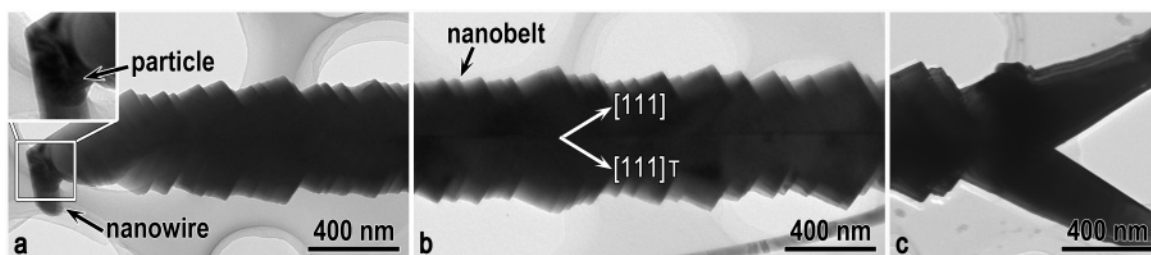
Figure 7. BF images of the ZnSe bicrystal nanobelt recorded at (a) the initial part, (b) the middle part, and (c) the end. The inset is the magnified BF image.

the orthotwin, which indicates that the rotation twinning is no longer equivalent to the mirror twinning in noncentral crystals. It is difficult to differentiate these two types by simple TEM techniques alone.[9] However, CBED method provides a useful route to detect the crystal polarity and thus understands the structural properties of planar defects in compound semiconductors.

To quantitatively determine the polarity of the bicrystal nanobelt, a CBED experiment is performed, and the results are presented in Figure 5. Viewed along the [$11\bar{2}$] axis, a BF image is obtained as shown in Figure 5c. Experimental CBED patterns recorded from each part are presented in Figure 5a,d, respectively, showing the polarity on the (111) surfaces. Moreover, the CBED patterns for ZnSe are also calculated using dynamic electron diffraction theory with the thicknesses of 212 and 228 nm, which are shown in Figure 5b,e, respectively. The excellent agreement between the experimental and the simulated results indicates that the polarity along the <111> direction is maintained in each part without reversal, which means that <111> twinning belongs to orthotwin (rotation twinning) while {113} is paratwin (mirror twinning). This result is reasonable on the basis of the viewpoint of energy, since the <111> rotation twinnings are expected to be of lower energy because of the absence of polarity reversal.[19] On the other hand, it is due to the polarity maintenance, as well as the chemical activity of Zn-terminated surface proposed by Wang et al.,[20] that the bicrystal nanobelt can keep a fast growth rate along the [111] direction.

Taking the polarity result into consideration, we can discuss the atomic model of the sample. Figure 6a is a mirror twinning model of the ZnSe bicrystal nanobelt, which is projected along the <112> axis. The twinning plane is {113} which is indicated by the dashed line; the bonds around the twinning plane are also drawn which implies the formation of homojunction. It is important to note that the polarity in each part of the nanobelt is maintained and the Zn-terminated {111} facets are also kept, which are consistent with CBED results shown in Figure 5a,d. On the other hand, a 180° rotation twinning model is also constructed to demonstrate the single part. Shown in Figure 6b,c are the atomic models viewed along the <112> and <110> axes, respectively. The {111} twinning plane is also indicated by the dashed line. It can be further confirmed in Figure 6b that the polarity remains the same when crossing the twinning plane, and the contrast provided by this model is homogeneous viewing along <112>, which is consistent with experimental result shown in Figure 1b. Moreover, all bonds across {111} twinning plane are also indicated in Figure 6c, which still remain the right Zn−Se bonds and consequently lower the system energy.[19] Meanwhile, by viewing along the <110> axis, the <111> rotation twinning can be clearly observed which also agrees with the SAED pattern in Figure 3c.

3.3. Formation of Bicrystal Nanobelts. We can discuss the formation of the ZnSe bicrystal nanobelts according to the

typical BF images in Figure 7. As described in section 2, the growth process can be divided into three stages, in which different reaction pressures are applied. On the basis of our previous investigations,[4,6] ZnSe nanowires will form in the first stage following the vapor−liquid−solid (VLS) mechanism,[21] which can be experimentally observed, and the remains of the nanowire is indicated by the arrowhead in Figure 7a. Moreover, as shown in the inset of Figure 7a, a particle can be observed at the end of the nanowire, which further confirms that the nanowire is guided by the VLS mechanism.[21]

In the second stage, the reaction pressure is changed immediately from 100 Torr to 0.02 Torr, hence, the growth is unstable. Because of the decreasing of the reaction pressure, the equilibrium vapor pressure will increase, and the nucleation will accelerate. Consequently, the size of the product will increase gradually, which is consistent with the morphology in Figure 7a. On the other hand, because of the position of the particle, the catalytic effect should be limited for the nanobelt growth; hence, the nanobelt is likely to grow according to the vapor−solid mechanism.[22]

In the last stage, the reaction pressure reaches equilibrium. According to the CBED results, each single plate will keep a fast but stable growth along its own [111] axis and thus form the bicrystal nanobelt, as shown in Figure 7b. Figure 7c shows a "V" shaped morphology, indicating the end of the growth.

4. Conclusions

In summary, novel zinc blende bicrystal nanobelts have been obtained. The {113} twinning filled with nanoscale <111> twinning lamellas is observed. The crystallographic relations of the bicrystal nanobelts are determined and the polarity along the <111> direction is examined which implies the absence of polarity reversal. The atomic model and the growth mechanism are also proposed on the basis of the polarity of the zinc blende ZnSe. This unusual structure offers a model system for further study of the structural, electrical, and optical properties and could lead to potential applications in nano-optoelectronics.

References and Notes

(1) Hu, J.; Odom, T. W.; Lieber, C. M. *Acc. Chem. Res.* **1999**, *32*, 435−445.

(2) Mo, M. S.; Zeng, J. H.; Liu, X. M.; Yu, W. C.; Zhang, S. Y.; Qian, Y. T. *Adv. Mater.* **2002**, *14*, 1658−1662.

{113} Twinned ZnSe Bicrystal Nanobelts

J. Phys. Chem. C, Vol. 112, No. 13, 2008 **4907**

(3) (a) Li, Q.; Gong, X. G.; Wang, C. R.; Wang, J.; Ip, K.; Hark, S. K. *Adv. Mater.* **2004**, *16*, 1436−1440. (b) Wang, Y. Q.; Philipose, U.; Xu, T.; Ruda, H. E.; Kavanagh, K. L. *Semicond. Sci. Technol.* **2007**, *22*, 175−178. (c) Zhang, Z. H.; Wang, F. F.; Duan, X. F. *J. Cryst. Growth* **2007**, *303*, 612−615.

(4) Leung, Y. P.; Choy, W. C. H.; Markov, I.; Pang, G. K. H.; Ong, H. C.; Yuk, T. I. *Appl. Phys. Lett.* **2006**, *88*, 183110.

(5) Liu, S. Y.; Choy, W. C. H.; Jin, L.; Leung, Y. P.; Zheng, G. P.; Wang, J. B.; Soh, A. K. *J. Phys. Chem. C* **2007**, *111*, 9055−9059.

(6) Jin, L.; Choy, W. C. H.; Leung, Y. P.; Yuk, T. I.; Ong, H. C.; Wang, J. B. *J. Appl. Phys.* **2007**, *102*, 044302.

(7) Bietsch, A.; Michel, B. *Appl. Phys. Lett.* **2002**, *80*, 3346−3348.

(8) Xu, L.; Su, Y.; Chen, Y. Q.; Xiao, H. H.; Zhu, L. A.; Zhou, Q. T.; Li, S. *J. Phys. Chem. B* **2006**, *110*, 6637−6642.

(9) Johansson, J.; Karlsson, L. S.; Svensson, C. P. T.; Martensson, T.; Wacaser, B. A.; Deppert, K.; Samuelson, L.; Seifert, W. *Nat. Mater.* **2006**, *5*, 574−580.

(10) Rujkorakarn, R.; Nelson, A. J. *J. Appl. Phys.* **2000**, *87*, 8557−8560.

(11) (a) Pässler, R.; Griebl, E.; Riepl, H.; Lautner, G.; Bauer, S.; Preis, H.; Gebhardt, W.; Buda, B.; As, D. J.; Schikora, D.; Lischka, K.; Papagelis, K.; Ves, S. *J. Appl. Phys.* **1999**, *86*, 4403−4411. (b) Haase, M. A.; Qiu, J.; DePuydt, J. M.; Cheng, H. *Appl. Phys. Lett.* **1991**, *59*, 1272−1274.

(12) Slobodskyy, A.; Gould, C.; Slobodskyy, T.; Becker, C. R.; Schmidt, G.; Molenkamp, L. W. *Phys. Rev. Lett.* **2003**, *90*, 246601.

(13) Panda, A. B.; Acharya, S.; Efrima, S. *Adv. Mater.* **2005**, *17*, 2471−2474.

(14) (a) Ohyama, T.; Sakakibara, K.; Otsuka, E.; Isshiki, M.; Igaki, K. *Phys. Rev. B* **1988**, *37*, 6153−6163. (b) Tomaru, T.; Ohyama, T.; Otsuka, E.; Isshiki, M.; Igaki, K. *Phys. Rev. B* **1992**, *46*, 9390−9399. (c) Hattori, R.; Fujii, K.; Ohyama, T.; Isshiki, M. *Physica E* **2006**, *32*, 237−240.

(15) Li, L. Y.; Wang, J. B.; Wang, R. H.; Liu, H. J.; Jia, C. L.; Ma, L. L.; Yu, Y. *Appl. Phys. Lett.* **2006**, *89*, 113109.

(16) (a) Mathur, N. D.; Burnell, G.; Isaac, S. P.; Jackson, T. J.; Teo, B. S.; MacManus-Driscoll, J. L.; Cohen, L. F.; Evetts, J. E.; Blamire, M. G. *Nature* **1991**, *387*, 266−268. (b) Mashtakov, A. D.; Konstantinyan, K. I.; Ovsyannikov, G. A.; Stephantsov, E. A. *Tech. Phys. Lett.* **1999**, *25*, 249−252. (c) Ataev, B. M.; Kamilov, I. K.; Mamedov, V. V.; Bagamadova, A. M.; Makhmudov, S. S. *J. Phys. D: Appl. Phys.* **2001**, *34*, L46−L47. (d) Xu, C. K.; Chun, J.; Rho, K.; Lee, H. J.; Jeong, Y. H.; Kim, D. E.; Chon, B.; Hong, S.; Joo, T. *Appl. Phys. Lett.* **2006**, *89*, 093117.

(17) (a) Dai, Y.; Zhang, Y.; Bai, Y. Q.; Wang, Z. L. *Chem. Phys. Lett.* **2003**, *375*, 96−101. (b) Meng, X. M.; Jiang, Y.; Liu, J.; Lee, C. S.; Bello, I.; Lee, S. T. *Appl. Phys. Lett.* **2003**, *83*, 2244−2246. (c) Chun, H. J.; Choi, Y. S.; Bae, S. Y.; Park, J. *Appl. Phys. A* **2005**, *81*, 539−542. (d) Yang, Z. X.; Zhu, F.; Wu, Y. J.; Zhou, W. M.; Zhang, Y. F. *Physica E* **2005**, *27*, 351−354.

(18) (a) Chou, C. T.; Cockayne, D. J. H.; Zou, J.; Kringhøj, P.; Jagadish, C. *Phys. Rev. B* **1995**, *52*, 17223−17230. (b) Goss, J. P.; Briddon, P. R.; Eberlein, T. A. G.; Jones, R.; Pinho, N.; Blumenau, A. T.; Öberg, S. *Appl. Phys. Lett.* **2004**, *85*, 4633−4635.

(19) Holt, D. B. *J. Mater. Sci.* **1984**, *19*, 439−446.

(20) Wang, Z. L.; Kong, X. Y.; Zuo, J. M. *Phys. Rev. Lett.* **2003**, *91*, 185502.

(21) Wagner, R. S.; Ellis, W. C. *Appl. Phys. Lett.* **1964**, *4*, 89−90.

(22) Jiang, Y.; Meng, X. M.; Yiu, W. C.; Liu, J.; Ding, J. X.; Lee, C. S.; Lee, S. T. *J. Phys. Chem. B* **2004**, *108*, 2784−2787.